Journal of Solid State Chemistry 260 (2018) 34–38

Contents lists available at ScienceDirect

Journal of Solid State Chemistry

journal homepage: www.elsevier.com/locate/jssc

Threshold heating temperature for magnetic hyperthermia: Controlling the heat exchange with the blocking temperature of magnetic nanoparticles

B. Pimentel[a], R.J. Caraballo-Vivas[a], N.R. Checca[a], V.I. Zverev[b,*], R.T. Salakhova[b], L.A. Makarova[b], A.P. Pyatakov[b], N.S. Perov[b], A.M. Tishin[b,c], A.A. Shtil[d], A.L. Rossi[e], M.S. Reis[a,f]

[a] Physics Institute, Fluminense Federal University, Av. Gal. Milton Tavares de Souza s/n, 24210-346 Niterói, RJ, Brazil
[b] Faculty of Physics, M.V. Lomonosov Moscow State University, 119991 Moscow, Russia
[c] Advanced Magnetic Technologies and Consulting LLC, 142190 Troitsk, Russia
[d] Blokhin National Medical Center of Oncology & Faculty of Chemistry, M.V. Lomonosov Moscow State University, 119991 Moscow, Russia
[e] Brazilian Center for Research in Physics, Rua Dr Xavier Sigaud 150, 22290-180 Rio de Janeiro, RJ, Brazil
[f] Physics Department and I3N, University of Aveiro, Aveiro 3810, Portugal

ARTICLE INFO

Keywords:
Magnetic nanoparticles
Hyperthermia
Self-controlled inductive heating
Self-regulating magnetic hyperthermia

ABSTRACT

$La_{0.75}Sr_{0.25}MnO_3$ nanoparticles with average diameter close to 20.9 nm were synthesized using a sol-gel method. Measurements showed that the heating process stops at the blocking temperaturesignificantly below the Curie temperature. Measurements of Specific Absorption Rate (SAR) as a function of AC magnetic field revealed a superquadratic power law, indicating that, in addition to usual Néel and Brown relaxation, the hysteresis also plays an important role in the mechanism of heating. The ability to control the threshold heating temperature, a low remanent magnetization and a low field needed to achieve the magnetic saturation are the advantages of this material for therapeutic magnetic hyperthermia.

1. Introduction

Cancer remains a major cause of death throughout the world [1]. New treatment modalities are aimed to improve the efficacy of tumor damage with minimal injury to surrounding tissues [2–6]. In this direction, physical methods using nanoparticles (NP) have been extensively studied in recent years [7]: in particular, development of magnetic NP for antitumor hyperthermia is under way [8–11]. This technique uses magnetic nanoparticles dispersed into a fluid (ferrofluid); then an external AC magnetic field (respecting the Brezovich limit [12]) is applied to heat the body or an area of the body.

Magnetic heating can be generated by three types of mechanisms: Néel relaxation, Brown relaxation, and hysteresis losses. For Néel relaxation, the magnetic moments of nanoparticles are consistently inverted due to AC magnetic field; energy is dissipated when the magnetic moments relax around the equilibrium position [8]. Brown relaxation presumes that, before the coherent reversal of magnetization (by Néel relaxation), the nanoparticles gain freedom of movement in the fluid due to external AC magnetic field [11]. The friction between the surface of nanoparticles and surrounding liquid causes heat release into the medium. The hysteresis losses are associated with the power dissipated in one cycle of magnetization [13,14].

A common parameter for quantitative characterization of magnetic hyperthermia is the Specific Absorption Rate (SAR). This value is of clinical importance for calculation of dose and duration of treatment [9]. It is generally believed that SAR optimization simply presumes an increase of its value. However, one can avoid tissue overheating that leads to an undesired side effect, by a *self-regulating (or self-controlled) hyperthermia* concept [15,16]. It consists of an internal mechanism that provides a high heating rate to the body and saturation of heating at higher temperatures. An obvious way is to use the ferromagnetic-paramagnetic phase transition: the temperature of NP heated under a magnetic field cannot exceed the Curie temperature [17,18]. Current materials are the superparamagnetic iron oxide NP; however, their Curie temperatures are far from what the clinical magnetic hyperthermia needs [19].

An alternative family of compounds for magnetic hyperthermia has been introduced [16,20–23], namely, $La_{1-x}Sr_xMnO_3$ (LSMO) NP. Physical parameters of these compounds such as Curie temperature, magnetic saturation and effective magnetic moment, can be easily managed. Therefore one can avoid overheating and damage of surrounding tissues. It is commonly supposed that the main factor limiting the excessive heating in magnetic NP (LSMO in particular) is the Curie temperature of the compound [17]. However, for magnetic

* Corresponding author.
E-mail addresses: vi.zverev@physics.msu.ru, bobzver@yandex.ru (V.I. Zverev).

https://doi.org/10.1016/j.jssc.2018.01.001
Received 4 September 2017; Received in revised form 16 December 2017; Accepted 2 January 2018
Available online 04 January 2018
0022-4596/

NP, other factors related to their nanoscale, such as superparamagnetism and, consequently, the blocking temperature, are also important. The aim of the present study is to identify other physical mechanisms related to NP that can control overheating. We herein report the preparation procedure and show that heating stops at the blocking temperature that differs significantly from the Curie temperature. Other parameters including the size of NP will be analyzed elsewhere.

The present study presents experimental details of sample preparation and SAR measurements, followed by a description of the crystal, morphology and magnetism. Section 4 discusses AC heating measurements and Section 5 summarizes our major findings.

2. Experimental details

A sol-gel method (Pechini) was employed to prepare LSMO NP. We used analytical quantities of lanthanum nitrate ($La(NO_3)_36H_2O$), strontium carbonate ($SrCO_3$) and manganese acetate ($Mn(CH_3COO)_24H_2O$). Individual reagents were dissolved in citric acid (with a molar ratio of 1:1 to cations) in deionized water and then mixed at 70 °C to obtain a transparent solution with molar ratio of La:Sr:Mn = 0.75:0.25:1. A suitable amount of ethylene glycol was added to the solution, with a molar ratio of 1:4 to citric acid [24]. The mixture was evaporated to get rid of excess of solvents and to promote polymerization, resulting in a brown viscous gel calcined at 700 °C for 4 h to obtain $La_{0.75}Sr_{0.25}MnO_3$ (LSMO) NP [25]. X-ray powder diffraction (XRD) data were collected at room temperature ($20° < 2\theta < 85°$ range, Bragg-Brentano geometry) on a Bruker AXS D8 Advance diffractometer with Cu-Kα radiation (λ = 1.54056 Å), 40 kV, 40 mA. Magnetic properties were investigated using a Lake Shore 7407 vibrating sample magnetometer in a magnetic field up to 1.6 T and 100–500 K temperature range. The experimental setup for calorimetric SAR measurements consists of an AC magnetic field module (the inner diameter of the coil is 7 mm), the temperature control system, the water cooling system and the external PC. There is a possibility to change the magnetic field amplitude in the range of 0–200 Oe and adjust the frequency in the vicinity of the coil resonance frequency, which is 100 kHz.

During the experiment, the test tube with LSMO NP suspended in water was placed inside the coil in a way that the center of the tube coincided with maximum field location. Magnetic field was switched on for a fixed time followed by measurement of induced heating (temperature change). SAR was calculated according to the equation:

$$SAR = C\frac{dT}{dt}\frac{M}{m} \quad (1)$$

where C is fluid (water+NP) heat capacity, $\frac{dT}{dt}$ is the rate of heating on the initial part of the curve, $\frac{M}{m}$ is ratio of the water mass to the mass of NP. Since the experimental conditions were non-adiabatic, it is necessary to take heat loss into account to get the correct value of . $\frac{dT}{dt}$ For this purpose, we measured the cooling curve after each heating cycle when the magnetic field was switched off. The power of heating corresponds to the sum of absolute values of derivatives $\frac{dT}{dt}$ of heating and cooling curves at the same temperature [26].

3. Crystal structure, morphology and magnetism

The X-ray diffractograms of the nanopowder confirmed the formation of a single phase LSMO sample, presenting the characteristic reflections of the compound (Fig. 1). The powder X-ray diffraction data were refined by Rietveld method using FullProf software. The system presents a perovskite structure at room temperature and pressure (space group R $\underline{3}$ C in a rhombohedral crystal system) [27].

The lattice parameters for this sample are: a = b = 5.5053 Å, c = 13.3864 Å, conforming cell volume of 351.3691 Å with reliability factor of χ^2 = 1.92. This is very close to the value observed in [28].

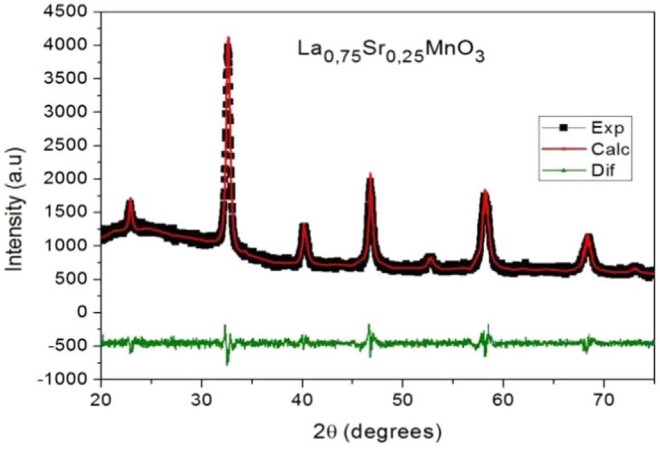

Fig. 1. X-ray diffraction pattern for $La_{0.75}Sr_{0.25}MnO_3$ (Cu conventional radiation: λ = 1.54056 Å). Black dots: experimental data; red line: theoretical data; green line: difference.

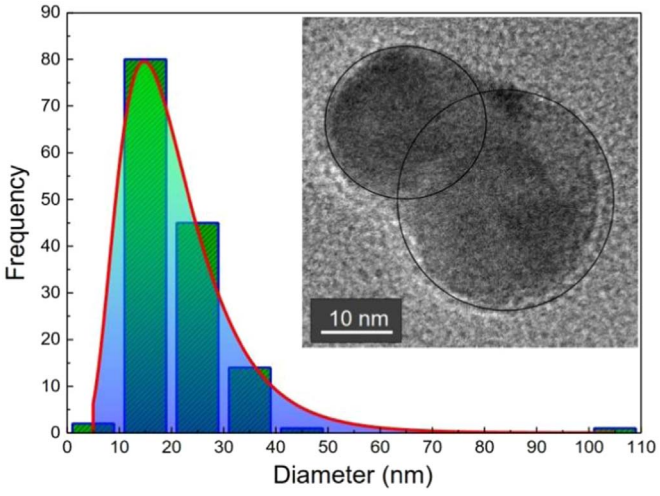

Fig. 2. NP size distribution based on several TEM imagesof transmission . Inset: typical NP.

Transmission Electron Microscopy (TEM) measurements were performed on a High Resolution Transmission Electron Microscope JEOL 2100F-200 kV at LABNANO - CBPF in order to confirm the particle size distribution (Fig. 2) and NP morphology. The distribution had high asymmetry; P thus we considered a lognormal distribution [29]:

$$f(D) = \frac{A}{\sigma D\sqrt{2\pi}} exp\left\{ - \frac{[ln(D)-\mu]^2}{2\sigma^2} \right\} \quad (2)$$

where D is NP size, and A is the amplitude of distribution. The mean size of NP <D> is defined by the parameters μ (location) and σ (scale) as:

$$<D> = exp\left\{\mu + \frac{\sigma^2}{2}\right\} \quad (3)$$

The most probable value of NP and standard deviation can be defined as:

$$D_m = exp\{\mu - \sigma\} \quad (4)$$

and

$$\Delta = \sqrt{exp\{\sigma^2\}-1} \cdot <D> \quad (5)$$

as well as the dimensionless skewness, that measures the asymmetry of distribution, assuming zero for a symmetric one:

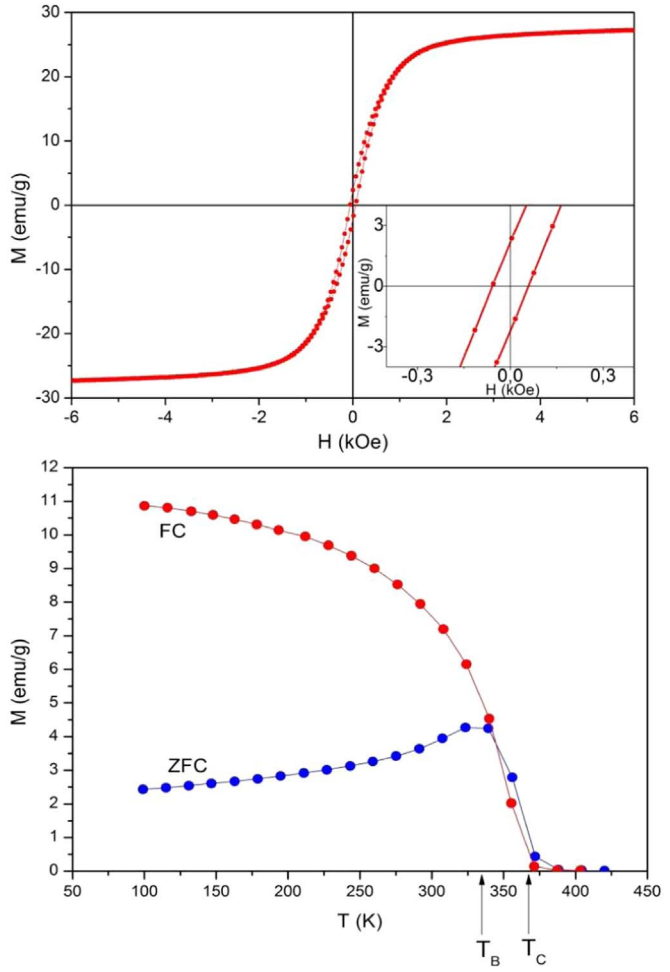

Fig. 3. Magnetic properties of LSMO. Top: M(H) curve at 300 K. See the hysteresis coming from the NP ensemble. Bottom: ZFC-FC curve. See the blocking and Curie temperature.

$$D_S = \sqrt{exp\{\sigma^2\}-1}\,(2+exp\{\sigma^2\}) \quad (6)$$

The values obtained from the fitting shown in Fig. 2 leads to: $<D> = 20.9nm$, $D_m = 16.6nm$, $\Delta = 10.6nm$ and $D_S = 1.7$.

We used Scherrer equation to reveal whether a single particle from TEM image corresponds to the single crystal. The equation gives the crystallite size [31]:

$$D_c = \frac{k\lambda}{\beta cos\theta}$$

where k is a dimensionless constant (close to 1), λ is the X-ray wavelength, θ is the diffraction angle of the most intense peak, and

$$\beta = \sqrt{Utan^2\theta + Vtan\theta + W}$$

is related to the full width at half maximum of the corresponding peak (for the present case: U = 0.1163, V = −0.5135 and W = 0.3871). The crystallite size was estimated as D_c = 18.4 nm, which is very close to the mean NP size of 20.9 nm obtained from TEM images. These results indicated that our NP are single crystals.

Magnetization as a function of magnetic field at 300 K is shown in Fig. 3-top panel where it is possible to observe the hysteresis. From this result we concluded that one mechanism of NP heating is hysteresis losses. By definition, superparamagnetic materials do not present hysteresis; however, hysteresis can occur with low remanent magnetization due to some bigger particles and agglomeration in the ensemble of NP [30]. For the present case, NP presented a remanent magnetization of M_R = 2.11 emu/g, which is appropriate for magnetic hyperthermia. Fig. 3-bottom panel shows ZFC-FC measurements where the blocking and critical temperatures T_B~335 K and T_c~367 K can estimated. These parameters were defined as maximum of ZFC curve and the inflexion point above T_B, respectively. Descriptions of the relationship between the magnetic properties of La-Sr and La-Ca NPs and their corresponding size have been published [25,31].

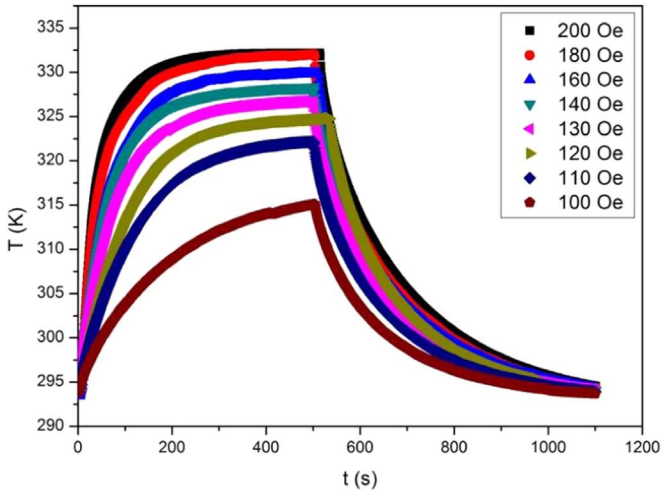

Fig. 4. Time course of AC magnetic-field heating (initial 500 s) and subsequent zero-field-cooling of LSMO NP for different values of field amplitude (frequency of AC field is 100 kHz). Note the saturation of maximum heating temperature within the field amplitude 180 Oe or higher.

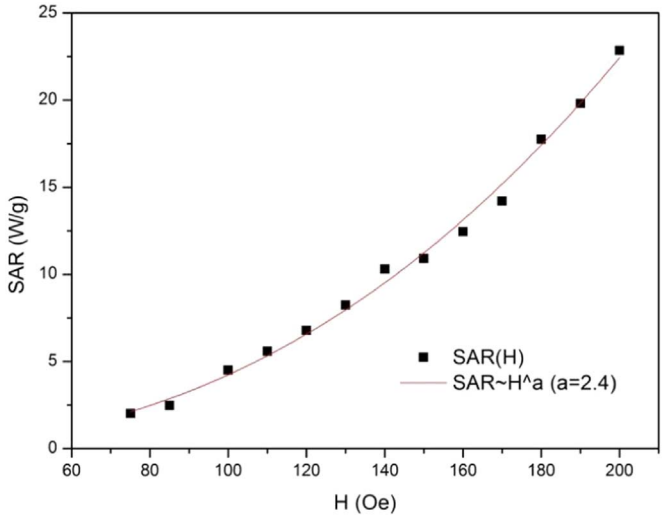

Fig. 5. SAR dependence on AC magnetic field amplitude for LSMO NP at room temperature 300 K.

4. AC magnetic field heating measurements

The results of heating/cooling of 20 mg LSMO NP, with average diameter of 20.9 nm, suspended in 100 ml water, are shown in Fig. 4. Once the frequency of AC field is fixed in the experiment, the dispersion of NP size and variation of magnetization relaxation time are not important for the amplitude dependence of magnetic heating (Fig. 4).

Heating demonstratedA the saturation in a temperature range of 333 K and higher. An AC field > 200 Oe is unable to change this maximum temperature. This effect is explained by magnetic relaxation behavior of NP below and above the blocking temperature at ~335 K. On the other hand, the initial heating rate (proportional to the initial slope of the curve in Fig. 4) increases by elevating the applied magnetic field even at high amplitudes.

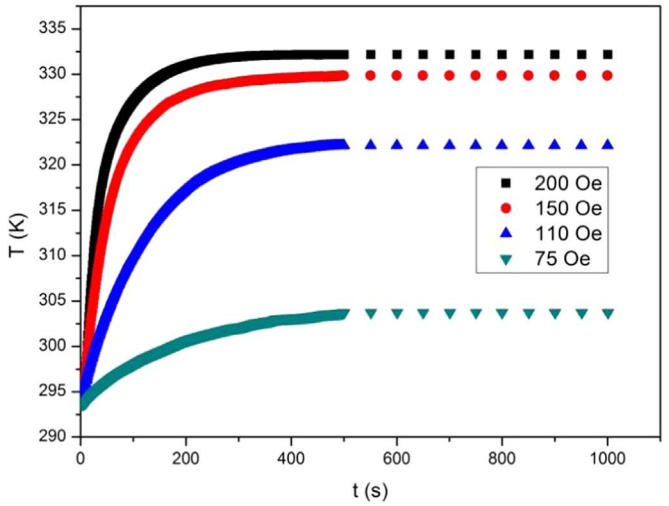

Fig. 6. Difference between temperature saturation time on heating for LSMO NP at various values of AC magnetic field amplitude.

Table 1
Heating parameters of LSMO NP obtained from approximation of curves in Fig. 3 by dependence of Eq. (7a). $\tau_{heating}$ and $\tau_{cooling}$ standing for τ_R in Eq. (7a).

Field (Oe)	$\tau_{heating}$(s)	$\tau_{cooling}$(s)	ΔT (K)	$\frac{dT}{dt}\left(\frac{K}{s}\right)$	SAR $\left(\frac{W}{g}\right)$
75	150	149	14	0.08	2.0
110	120	146	31	0.22	5.6
150	58	152	39	0.43	10.9
200	39	160	42	0.91	23.0

Fig. 5 shows the dependence of SAR (calculated from Eq. (1) and the slope curves in Fig. 4 - m = 0.1 g, M = 20 mg, C = 4.2 J/g) on the AC magnetic field amplitude. It is known that the dependence of SAR on the AC magnetic field amplitude for superparamagnetic NP (where relaxation heating mechanism prevails over the hysteresis) has a quadratic dependence [32–34]. Thus, a power law of the kind $SAR \sim H^a$ was fitted to the experimental data (the brown line in Fig. 5) where we found a slightdeviation from the quadratic law. In fact, we found a superquadratic power with $a = 2.4$ suggesting that the mechanism of heating is not limited solely to relaxation (Brown and Néel) [32]. A contribution of hysteresis losses should also be considered below the blocking temperature $T_B \sim 335$ K.

It is important to notice that the stop of heating corresponds to the blocking temperature. This can explain the fact that the elevation of the initial heating rate (dT/dt) by increasing the AC magnetic field amplitude is not accompanied by the growth of final heating (ΔT), which is observed for conventional time evolution of temperature:

$$T(t) = T_0 + \Delta T \cdot (1 - exp(-t/\tau_R)) \quad (7)$$

$$\Delta T = \frac{dT}{dt}(T = T_0) \cdot \tau_R \quad (8)$$

where T_0 is the initial temperature of the experiment, and τ_R is the relaxation constant which depends on heat capacity, the surface of the sample, and the heat transfer coefficient between the sample and the medium [35].

In the low magnetic field range (< 110 Oe) the Eqs. (7) well describe the heating and cooling processes. However, as soon as the maximum heating temperature approaches the blocking values, the model with constant τ_R fails to adequately describe the heating process: its approximation by Eq. (7a) gives the characteristic time (stands for τ_R in Eq. (7a)) that decreases with magnetic field amplitude. This is obvious if one compares the heating curves at 75 Oe and 200 Oe (Fig. 6). According to thermodynamics, it should not depend on field value; indeed, the characteristic cooling time (standing for τ_R in Eq. (7a) when the field is switched off) is nearly the same for all curves (~150 s) as the conventional thermodynamic relaxation time τ_R should be. The heating parameters are presented in Table 1.

5. Conclusions

A reproducible procedure of preparation of $La_{0.75}Sr_{0.25}MnO_3$ magnetic NP was developed. We obtained NP with average diameter about 20.9 nm, a blocking temperature close to 335 K and Curie temperature at 367 K. The hyperthermia experiments confirmed that the heating process stops at the blocking temperature significantly below Curie temperature. SAR as a function of AC magnetic field provided a superquadratic power law, indicating that, in addition to Néel and Brown relaxation, the hysteresis is also important in the mechanism of heating.

Our results provide evidence that this material is applicable for magnetic hyperthermia due to heating control by means of a threshold temperature, a self-stopping mechanism. This mechanism is valuable in the clinic since it minimizes the risk of overheating.

Acknowledgements

BP, RJCV and MSR thank Brazilian agencies CNPq, CAPES, FAPERJ and PROPPI-UFF for financial support. MSR belongs to the INCT of “Refrigeração e Termofísica”, funding by CNPq under grant number 465448/2014-3. This work was also funded by FEDER through the COMPETE 2020 Programme and National Funds through FCT - Portuguese Foundation for Science and Technology under the project UID/CTM/50025/2013. The authors thank Radel Gimaev and Vladimir Markov for assistance with experiments.

References

[1] D. Max. Parkin, F. Bray, J. Ferlay, P. Pisani, J. Clin. 55 (2005) 2.
[2] C. Huang, Z. Tang, Y. Zhou, X. Zhou, Y. Jin, D. Li, Y. Yang, S. Zhou, Int. J. Pharm. 429 (2012) 113.
[3] C.-J. Jia, L.-D. Sun, F. Luo, X.-D. Han, L.J. Heyderman, Z.-G. Yan, C.-H. Yan, K. Zheng, Z. Zhang, M. Takano, et al., J. Am. Chem. Soc. 130 (2008) 16968.
[4] A. Jordan, P. Wust, H. Fähling, W. John, A. Hinz, R. Felix, Int. J. Hyperth. 25 (2009) 499.
[5] J. Dobson, Nat. Mater. 9 (2010) 95.
[6] J. Carrey, B. Mehdaoui, M. Respaud, J. Appl. Phys. 109 (2011) 083921.
[7] I. Brigger, C. Dubernet, P. Couvreur, Adv. Drug Deliv. Rev. 54 (2002) 631.
[8] N. Prasad, K. Rathinasamy, D. Panda, D. Bahadur, J. Biomed. Mater. Res. Part B: Appl. Biomater. 85 (2008) 409.
[9] S. Vasseur, E. Duguet, J. Portier, G. Goglio, S. Mornet, E. Hadová, K. Knízek, M. Marysko, P. Veverka, E. Pollert, J. Magn. Magn. Mater. 302 (2006) 315.
[10] N. Thorat, V. Khot, A. Salunkhe, R. Ningthoujam, S. Pawar, Colloids Surf. B: Biointerfaces 104 (2013) 40.
[11] S. Mornet, S. Vasseur, F. Grasset, P. Veverka, G. Goglio, A. Demourgues, J. Portier, E. Pollert, E. Duguet, Prog. Solid State Chem. 34 (2006) 237.
[12] I.A. Brezovich, Med. Phys. Monogr. 16 (1988) 82.
[13] N.K. Prasad, L. Hardel, E. Duguet, D. Bahadur, J. Magn. Magn. Mater. 321 (2009) 1490.
[14] G. Bertotti, Hysteresis in Magnetism: For Physicist, Materials Scientist, and Engineers, Academic Press, 1998.
[15] H. Saito, K. Mitobe, A. Ito, Y. Sugawara, K. Maruyama, Y. Minamiya, S. Motoyama, N. Yoshimura, J. Ogawa, Cancer Sci. 99 (2008) 805.
[16] A.A. Kuznetsov, O.A. Shlyakhtin, N.A. Brusentov, O.A.O. Kuznetsov, Eur. Cells Mater. 3 (2002) 75.
[17] K.L. McNerny, Y. Kim, D.E. Laughlin, M.E. McHenry, J. Appl. Phys. 107 (2010) 09A312.
[18] H. Hejase, S.S. Hayek, S. Qadri, Y. Haik, J. Magn. Magn. Mater. 324 (2012) 3620.
[19] E. Pollert, P. Veverka, M. Veverka, O. Kaman, K. Záveta, S. Vasseur, R. Epherre, G. Goglio, E. Duguet, Prog. Solid State Chem. 37 (2009) 1.
[20] R. Epherre, E. Duguet, S. Mornet, E. Pollert, S. Louguet, S. Lecommandoux, C. Schatz, G. Goglio, J. Mater. Chem. 21 (2011) 4393.
[21] E. Natividad, M. Castro, G. Goglio, I. Andreu, R. Epherre, E. Duguet, A. Mediano,

Nanoscale 4 (2012) 3954.
[22] E. Pollert, K. Knizek, M. Marysko, P. Kaspar, S. Vasseur, E. Duguet, J. Magn. Magn. Mater. 316 (2007) 122.
[23] M.H. Ehsani, P. Kameli, M.E. Ghazi, F.S. Razavi, M. Taheri, J. Appl. Phys. 114 (2013) 223907.
[24] W.L. Tai, A.P. Lessing, J. Mater. Res. 7 (1992) 502.
[25] V.M. Andrade, R.J. Caraballo Vivas, S.S. Pedro, J.C.G. Tedesco, A.L. Rossi, A.A. Coelho, D.L. Rocco, M.S. Reis, Acta Mater. 102 (2016) 49.
[26] N. Iacob, G. Schinteie, P. Palade, C. Ticos, V. Kuncser, Eur. Phys. J. E 38 (2015) 57.
[27] D.-H. Ji, X. Hou, G.-D. Tang, Z.-Z. Li, D.-L. Hou, M.-G. Zhu, Rare Met. 33 (2014) 452.
[28] H. Qin, J. Hu, J. Chen, Y. Wang, Z. Wang, J. Appl. Phys. 91 (2002) 10003.
[29] L.C. Branquinho, M.S. Carriao, A.S. Costa, N. Zufelato, M.H. Sousa, R. Miotto, R. Ivkov, A.F. Bakuzis, Sci. Rep. 3 (2013) 2887.
[30] M. Mahmoudi, A. Simchi, M. Imani, A. Milani, P. Stroeve, J. Phys. Chem. B 112 (2008) 46.
[31] V.M. Andrade, R.J. Caraballo-Vivas, T. Costas-Soares, S.S. Pedro, D.L. Rocco, M.S. Reis, A.P.C. Campos, A.A. Coelho, J. Solid State Chem. 219 (2014) 87.
[32] R.E. Rosensweig, J. Magn. Magn. Mater. 252 (2002) 370.
[33] G. Landi, J. Magn. Magn. Mater. 326 (2013) 14.
[34] K. Murase, H. Takata, Y. Takeuchi, S. Saito, Phys. Med. 29 (2013) 624.
[35] E.A. Périgo, G. Hemery, O. Sandre, D. Ortega, E. Garaio, F. Plazaola, F.J. Teran, Appl. Phys. Rev. 2 (2015) 041302.